The use of the adding-doubling method for the optical optimization of planar luminescent down shifting layers for solar cells

Sven Leyre,[1,2,3,*] Jan Cappelle,[4] Guy Durinck,[1,3] Aimi Abass,[5] Johan Hofkens,[6] Geert Deconinck,[2] and Peter Hanselaer[1,3]

[1]*Light & Lighting Laboratory, KU Leuven, Gebroeders Desmetstraat 1, 9000 Gent, Belgium*
[2]*ESAT/ELECTA, KU Leuven, Kasteelpark Arenberg 10, bus 2445, 3001 Leuven, Belgium*
[3]*SIM (Flemish Strategic Initiative on Materials), SOPPOM program, Technologiepark 935, 9052 Zwijnaarde, Belgium*
[4]*E&A, KU Leuven, Gebroeders Desmetstraat 1, 9000 Gent, Belgium*
[5]*Electronics and Information Systems (ELIS), Ghent University, Sint-Pietersnieuwstraat 41, 9000 Gent, Belgium*
[6]*Departement of Chemistry, KU Leuven, Celestijnenlaan 200 F, bus 2404, Leuven 3001, Belgium*
[*]*sven.leyre@kuleuven.be*

Abstract: To enhance the efficiency of solar cells, a luminescent down shifting layer can be applied in order to adapt the solar spectrum to the spectral internal quantum efficiency of the semiconductor. Optimization of such luminescent down shifting layers benefits from quick and direct evaluation methods. In this paper, the potential of the adding-doubling method is investigated to simulate the optical behavior of an encapsulated solar cell including a planar luminescent down shifting layer. The results of the adding-doubling method are compared with traditional Monte Carlo ray tracing simulations. The average relative deviation is found to be less than 1.5% for the absorptance in the active layer and the reflectance from the encapsulated cell, while the computation time can be decreased with a factor 52. Furthermore, the adding-doubling method is adopted to investigate the suitability of the SrB4O7:5%Sm2 + ,5%Eu2 + phosphor as a luminescent down shifting material in combination with a Copper Indium Gallium Selenide solar cell. A maximum increase of 9.0% in the short-circuit current can be expected if precautions are taken to reduce the scattering by matching the refractive index of host material to the phosphor particles. To be useful as luminescent down shifting material, the minimal value of the quantum yield of the phosphor is determined to be 0.64.

OCIS codes: (080.1753) Computation methods; (350.6050) Solar energy; (260.2510) Fluorescence.

References and links

1. W. G. J. H. M. van Sark, "Enhancement of solar cell performance by employing planar spectral converters," Appl. Phys. Lett. **87**(15), 151117 (2005).
2. E. Klampaftis, D. Ross, S. Seyrling, A. N. Tiwari, and B. S. Richards, "Increase in short-wavelength response of encapsulated CIGS devices by doping the encapsulation layer with luminescent material," Sol. Energy Mater. Sol. Cells **101**, 62–67 (2012).
3. P. Chung, H.-H. Chung, and P. H. Holloway, "Phosphor coatings to enhance Si photovoltaic cell performance," J. Vac. Sci. Technol. A **25**(1), 61–66 (2007).
4. W. G. J. H. M. van Sark, A. Meijerink, R. E. I. Schropp, J. A. M. van Roosmalen, and E. H. Lysen, "Enhancing solar cell efficiency by using spectral converters," Sol. Energy Mater. Sol. Cells **87**(1-4), 395–409 (2005).
5. H. J. Hovel, R. T. Hodgson, and J. M. Woodall, "The effect of fluorescent wavelength shifting on solar cell spectral response," Sol. Energy Mater. **2**(1), 19–29 (1979).
6. B. S. Richards and K. R. McIntosh, "Overcoming the poor short wavelength spectral response of CdS/CdTe photovoltaic modules via luminescence down-shifting: Ray-Tracing Simulations," Prog. Photovolt. Res. Appl. **15**(1), 27–34 (2007).
7. E. Klampaftis and B. S. Richards, "Improvement in multi-crystalline silicon solar cell efficiency via addition of luminescent material to EVA encapsulation layer," Prog. Photovolt. Res. Appl. **19**(3), 345–351 (2011).

#199984 - $15.00 USD Received 22 Oct 2013; revised 18 Jan 2014; accepted 26 Jan 2014; published 1 Apr 2014

8. C. del Cañizo, I. Tobías, J. Pérez-Bedmar, A. C. Pan, and A. Luque, "Implementation of a Monte Carlo method to model photon conversion for solar cells," Thin Solid Films **516**(20), 6757–6762 (2008).
9. E. Klampaftis, D. Ross, K. R. McIntosh, and B. S. Richards, "Enhancing the performance of solar cells via luminescent down-shifting of the incident spectrum: A review," Sol. Energy Mater. Sol. Cells **93**(8), 1182–1194 (2009).
10. J. Chen and X. Intes, "Comparison of Monte Carlo methods for fluorescence molecular tomography-computational efficiency," Med. Phys. **38**(10), 5788–5798 (2011).
11. G. G. Stokes, "On the intensity of the light reflected from or transmitted through a pile of plates," Proc. R. Soc. Lond. **11**(0), 545–556 (1860).
12. W. J. Wiscombe, "On initialization, error and flux conservation in the doubling method," J. Quant. Spectrosc. Radiat. Transf. **16**(8), 637–658 (1976).
13. J. E. Hansen, "Radiative transfer by doubling very thin layers," Astrophys. J. **155**, 565–573 (1969).
14. S. A. Prahl, M. J. C. van Gemert, and A. J. Welch, "Determining the optical properties of turbid mediaby using the adding-doubling method," Appl. Opt. **32**(4), 559–568 (1993).
15. W. Saeys, M. A. Velazco-Roa, S. N. Thennadil, H. Ramon, and B. M. Nicolaï, "Optical properties of apple skin and flesh in the wavelength range from 350 to 2200 nm," Appl. Opt. **47**(7), 908–919 (2008).
16. J. W. Pickering, S. A. Prahl, N. van Wieringen, J. F. Beek, H. J. C. M. Sterenborg, and M. J. C. van Gemert, "Double-integrating-sphere system for measuring the optical properties of tissue," Appl. Opt. **32**(4), 399–410 (1993).
17. S. Leyre, G. Durinck, B. Van Giel, W. Saeys, J. Hofkens, G. Deconinck, and P. Hanselaer, "Extended adding-doubling method for fluorescent applications," Opt. Express **20**(16), 17856–17872 (2012).
18. K. R. McIntosh, J. N. Cotsell, A. W. Norris, N. E. Powell, and B. M. Ketola, "An optical comparison of silicone and EVA encapsulants for conventional silicon PV modules: A ray-tracing study," in *Proceedings of the 34th IEEE Photovoltaic Specialists Conference* (Philadelphia, 2009), pp. 544–549.
19. P. K. Johnson, A. O. Pudov, J. R. Sites, K. Ramanathan, F. S. Hasoon, and D. E. Tarrant, "Interface properties of CIGS(S)/buffer layers formed by the Cd-partial electroyle process," in Proceedings of the 29th IEEE Photovoltaic Specialists Conference (New Orleans, 2002), pp. 1–4.
20. C. Battaglia, M. Boccard, F.-J. Haug, and C. Ballif, "Light trapping in solar cells: When does a Lambertian scatterer scatter Lambertianly?" J. Appl. Phys. **112**(9), 094504 (2012).
21. D. K. G. de Boer, D. J. Broer, M. G. Debije, W. Keur, A. Meijerink, C. R. Ronda, and P. P. C. Verbunt, "Progress in phosphors and filters for luminescent solar concentrators," Opt. Express **20**(S3), A395–A405 (2012).
22. Z. Liu, S. Liu, K. Wang, and X. Luo, "Measurement and numerical studies of optical properties of YAG:Ce phosphor for white light-emitting diode packaging," Appl. Opt. **49**(2), 247–257 (2010).
23. L. Junyuan, R. Haibo, W. Wei, W. Xianlong, Z. Linsong, Z. Da, W. Xuemei, and L. Qiaolin, "Optical simulation of phosphor layer of white LEDs," J. Semicond. **34**(5), 053008 (2013).
24. J. H. Joseph, W. J. Wiscombe, and J. A. Weinman, "The Delta-Eddington Approximation for radiative flux transfer," J. Atmos. Sci. **33**(12), 2452–2459 (1976).
25. J.-G. Liu and M. Ueda, "High refractive index polymers: fundamental research and practical applications," J. Mater. Chem. **19**(47), 8907–8919 (2009).
26. I. Denisyuk and M. Fokina, "A review of high nanoparticles concentration composites: Semiconductor and high refractive index materials," in *Nanocrystals*, Y. Masuda, Ed. (InTech, 2010), pp. 109–142.
27. T. C. Choy, Effective Medium Theory: Principles and Applications. (Oxford: Clarendon Press, 1999).
28. P. Tao, Y. Li, A. Rungta, A. Viswanath, J. Gao, B. C. Benicewicz, R. W. Siegela, and L. S. Schadler, "TiO2 nanocomposites with high refractive index and transparency," J. Mater. Chem. **21**(46), 18623–18629 (2011).
29. C. Lü, Z. Cui, Z. Li, B. Yang, and J. Shen, "High refractive index thin films of ZnS/polythiourethane nanocomposites," J. Mater. Chem. **13**(3), 526–530 (2003).
30. D. Şahin and B. Ilan, "Radiative transport theory for light propagation in luminescent media," J. Opt. Soc. Am. A **30**(5), 813–820 (2013).
31. D. Yudovsky and L. Pilon, "Modeling the local excitation fluence rate and fluorescence emission in absorbing and strongly scattering multilayered media," Appl. Opt. **49**(31), 6072–6084 (2010).
32. A. Joshi, J. C. Rasmussen, E. M. Sevick-Muraca, T. A. Wareing, and J. McGhee, "Radiative transport-based frequency-domain fluorescence tomography," Phys. Med. Biol. **53**(8), 2069–2088 (2008).

1. Introduction

In the last decades, a lot of research efforts have been spent to improve solar cell efficiency by introducing a luminescent down shifting layer on top of the cell [1–9]. The luminescent down shifting (LDS) layer absorbs photons in the short wavelength range of the solar spectrum where the response of the solar cell is rather poor, and converts the photons to longer wavelengths where the solar cell is more efficient, thus improving the overall efficiency of the solar cell.

Depending on the specific combination of luminescent down shifting material, the type of solar cell and the specific configuration, a broad range of efficiency increases can be obtained. For almost all types of solar cells, an efficiency improvement has been reported

#199984 - $15.00 USD Received 22 Oct 2013; revised 18 Jan 2014; accepted 26 Jan 2014; published 1 Apr 2014

when an appropriate luminescent down shifting layer is applied, up until + 39% and + 50% for CdTe and a-Si type solar cells, respectively [9]. For Copper Indium Gallium Selenide (CIGS) solar cells an efficiency increase of 1-4% has been reported in literature [2,9].

Usually the optimization of such a LDS layer is tackled with Monte Carlo ray tracing simulations [6–8]. The disadvantage of these kind of simulations is that they can take up a large amount of computation time [10], especially when layered media with multiple Fresnel reflections or media containing scattering particles have to be simulated. This time consuming method hampers an efficient optimization procedure.

To decrease the computation time and provide an efficient optimization tool, the adding-doubling (AD) method is proposed. The AD method was first introduced by Stokes as a method to calculate the transmission through a pile of plates [11]. Using the transmission and reflection characteristics of two slabs of material as input, the transmission and reflection characteristics of the combination of the two materials is calculated [11–13]. The method is especially suited to describe stacks of scattering layers of infinite lateral dimensions. The method became popular in the astronomy field, where it was useful the determine the transmission and scattering in the galaxies and through clouds [12,13]. The AD algorithm is also applied in the biomedical field as an inverse procedure to estimate optical properties of tissues [14–16]. Recently the AD method was extended and successfully validated for fluorescent applications [17].

The AD method is a vector-matrix method to solve the radiative transfer equation, which describes the light propagation through a medium. The light incident on the material is divided into angular subdivisions, called channels, and can be written as a vector, where each element in the vector represents the flux within one channel. Reflection and transmission events are represented as matrices, allowing angular redistribution of the light (e.g. due to scattering). Conversion matrices can be used to redistribute the light over different wavelengths. Calculating the light transport through a layer is reduced to a simple matrix operation. A more elaborate discussion of the AD method can be found in the Appendix and in ref [17].

The AD method is well suited to implement the geometry of an encapsulated solar cell, which usually consists of several layers deposited on top of each other. A disadvantage of the method is that the losses through the sides of the layers cannot be simulated. However, if the layers are reasonably thin compared to the surface area, which is usually the case in solar cells, these effects are expected to be negligible. For more complex geometries such as non-azimuthally symmetric configurations, the Monte Carlo method remains a better choice.

In this paper, the AD method is applied for the simulation of the optical behavior of an encapsulated solar cell including a LDS layer. The results are compared to the results obtained with traditional Monte Carlo simulations. Next, the LDS layer is optimized by adjusting the concentration of SrB_4O_7:5%Sm^{2+},5%Eu^{2+} phosphor in the encapsulation layer and using the quantum yield of the phosphor as an additional parameter. The impact on the short circuit current of encapsulated CIGS solar cell is investigated.

2. Simulation geometry

The simulations are performed for a CIGS solar cell encapsulated with a multi-layer ethylene-vinyl acetate (EVA) coating and a glass cover. CIGS solar cells exhibit typically a poor short-wavelength response and offer thus a large potential for improvement through the use of a LDS layer [2]. The geometry of the encapsulated solar cell considered in this paper is represented in Fig. 1, the glass cover has a thickness of 3 mm, the top and bottom EVA layer have a thickness of 175 μm, the LDS layer has a thickness of 100 μm.

#199984 - $15.00 USD Received 22 Oct 2013; revised 18 Jan 2014; accepted 26 Jan 2014; published 1 Apr 2014

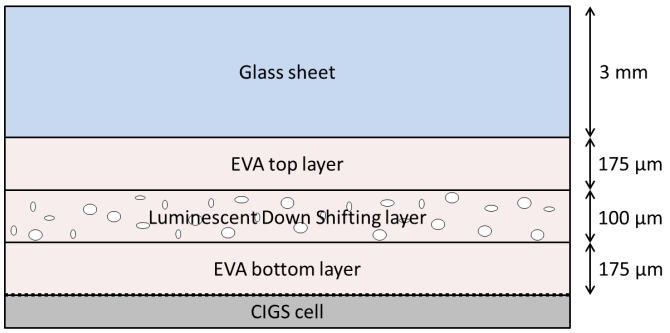

Fig. 1. Encapsulation geometry used for simulations (dimensions not to scale).

The refractive indices of the EVA sheet and the low-iron glass cover were taking from [18]. The absorption coefficients of the EVA sheet and glass cover were determined by transmission measurements. Commercial EVA sheets usually include uv blockers, which absorb radiation below 380 nm in order to prevent the material to degrade. Since this hampers the potential increase in efficiency by the LDS layer, an EVA sheet without uv blockers was used in our simulations. Alternative measures to protect the layers from uv induced degradation must be taken, e.g. with uv stabilizers such as hindered amine light stabilizers (HALS). The spectral transmittance of an EVA sheet with and without uv blockers and low-iron glass is given in Fig. 2.

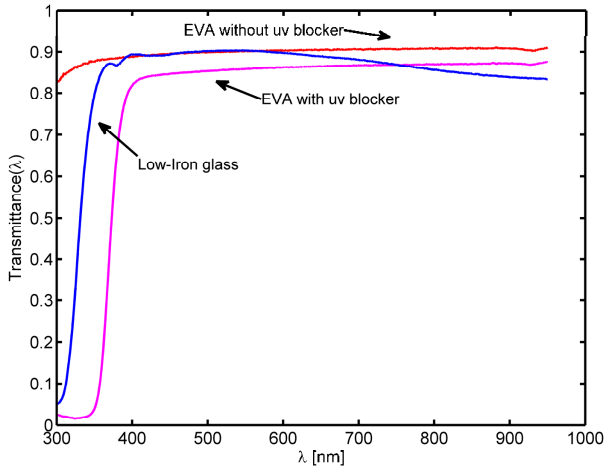

Fig. 2. Transmittance spectra of Low-Iron Glass (blue) and EVA with (magenta) and without (red) uv blocker.

The reflectance properties and internal quantum efficiency (IQE) of the CIGS solar cell are taken from [19] and are represented in Fig. 3. Since no information on the angular distribution of the reflectance of the cell is available, a Lambertian reflection pattern is assumed, which is a reasonable assumption for textured solar cells [20]. The light propagation through the different layers of the CIGS solar cell is not investigated, only the reflection from the complete cell is taken into account.

#199984 - $15.00 USD Received 22 Oct 2013; revised 18 Jan 2014; accepted 26 Jan 2014; published 1 Apr 2014

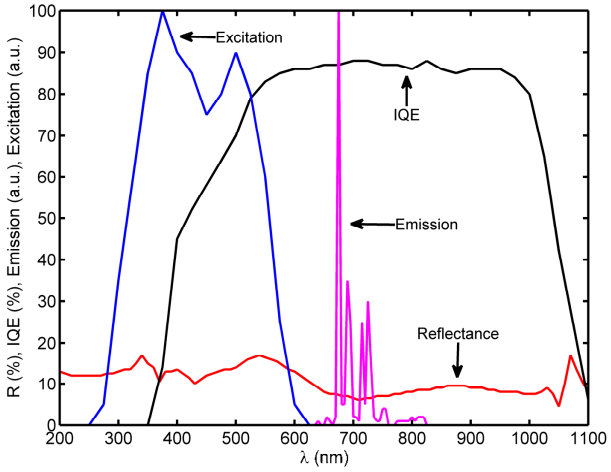

Fig. 3. Reflectance (red) and IQE (black) of the CIGS cell, together with the excitation (blue) and emission spectrum (magenta) of the SrB_4O_7:5%Sm^{2+},5%Eu^{2+} phosphor.

From Fig. 3, it can be seen that the IQE of the CIGS cell is very low below 400 nm, and reaches its maximum between 600 and 900 nm. As luminescent material, the rare earth phosphor SrB_4O_7:5%Sm^{2+},5%Eu^{2+} is chosen, which has a high quantum yield and a wide excitation spectrum between 250 and 600 nm and an emission spectrum between 650 and 850 nm [21]. The excitation and emission spectra are also represented in Fig. 3.

It can be noted that the phosphor absorbs most of the radiation in the region where the solar cell has a lower IQE. The absorption coefficient at 500 nm of the phosphor at a concentration of 3 vol% in EVA is approximately 3.0 mm^{-1} [21] and the scattering properties of the phosphor embedded in EVA are determined through Lorenz-Mie calculations. The refractive index of the phosphor particles and EVA is taken to be 1.74 and 1.49, respectively [21]. The average diameter of the particles is 5 µm, with a normal particle size distribution characterized by σ = 1 µm [21]. This results in an average scattering coefficient $\mu_s \approx 20.5$ mm^{-1} over the 280-1200 nm wavelength range and an average anisotropy factor $g \approx 0.905$. The scattering coefficient (μ_s) defines the probability of a photon to be scattered after travelling a unit path length through the material. The anisotropy factor (g) represent the average cosine of the angle between incident and scattered direction. This factor can take values from −1 to 1, with values lower and higher than 0 indicating preferential backward scattering and forward scattering, respectively. The anisotropy factor g is determined from the phase function obtained using the Lorenz-Mie calculations.

The reflectance from the encapsulated cell and the absorptance within the semiconductor material are simulated for the stack described above. The IQE data are applied to the photons which are not reflected by the semiconductor.

3. Adding-doubling vs Monte Carlo simulations: accuracy and computation time comparison

To validate the AD method for the simulation of the solar cell geometry described in the previous section, results obtained with AD will be compared with the results obtained with the traditional Monte Carlo ray tracing, commonly used for the optical simulation of LDS layers [7,8].

The Monte Carlo (MC) simulations are done using the commercial software package TracePro® 7.3. In this package, regular reflections are handled by attributing a probability to each ray to be reflected or transmitted at an interface according to the Fresnel reflection and transmission coefficients. The volume scattering is handled by use of the scattering

#199984 - $15.00 USD Received 22 Oct 2013; revised 18 Jan 2014; accepted 26 Jan 2014; published 1 Apr 2014

coefficient and the anisotropy factor, which can be introduced in the program for each wavelength. The software allows the choice of 3 phase functions (which determines the probability of a photon to be scattered in a given direction after a single scatter event): the Henyey-Greenstein phase function, the Gegenbauer phase function or a user defined phase function. In all our simulations, the Henyey-Greenstein phase function was selected. This phase function is commonly used as alternative for the more complex Mie phase function [22,23] and allows an easy integration in the adding-doubling algorithm [24]. To handle the fluorescence, a two stage ray tracing procedure is implemented: first all rays from the original source are traced through the geometry and rays absorbed in the fluorescent component are stored. Next, a second ray trace is performed starting with the rays emitted by the fluorescent component as source.

For the AD method, the solar cell geometry discussed in the previous section, is divided into 4 macroscopic layers of which the reflection and transmission characteristics must be determined: the glass cover and the 3 EVA layers. The CIGS cell itself is not a part of the model, since only the macroscopic reflectance at the encapsulant-cell interface is taken into account. In addition to the 4 layers, 5 interfaces between the different media have to be taken into account: air-glass, glass-top EVA layer, top EVA layer-LDS layer, LDS layer-bottom EVA layer and bottom EVA layer-CIGS cell, these interfaces are taken into account as separate layers in the AD method.

The reflection from the total stack and the absorption in the CIGS cell were investigated. The simulation was performed from 280 nm until 1200 nm in steps of 5 nm, resulting in 185 incident wavelengths to be simulated. The incident direction of the radiation was assumed to be perpendicular to the solar cell, the spectrum was chosen to be the AM1.5 standard solar spectrum.

3.1 Accuracy comparison

Using an infinite number of rays in the MC simulations, would result in the perfect solution of the light propagation problem. Using a smaller amount of rays will introduce some noise in the simulations. To estimate the accuracy of the AD method, the MC ray trace was performed with 10000 rays per wavelength. This resulted in an average relative standard deviation over all wavelengths of 0.5% between traces performed with different random seeds.

Since the AD method assumes infinite plane parallel layers and therefore light escaping from the edges of the cell is not taken into account. To mimic this situation in the ray tracing geometry, the diameter of the solar cell used in the MC simulations was taken to be 1000 mm and a diameter of 10 mm was attributed to the incident beam.

In Fig. 4, the absorption in the CIGS layer and the reflected irradiance of the solar cell are shown for both MC simulations and AD calculations. The average relative deviation over all wavelengths between both approaches is lower than 0.5% when using 32 channels and lower than 1% when using 16 channels (not shown on figure).

The absorption shows multiple peaks at certain wavelengths between 600 and 800 nm reaching higher than the incident irradiance (see Fig. 4). This is due to the fluorescence in the LDS layer, where light between 300 and 600 nm is converted to the 600 and 800 nm, resulting in more power at those wavelengths than originally present in the incident spectrum (and thus explaining the absorption to be larger than the incident irradiance). Although the fluorescence occurs isotropically, it can be seen that most of the converted light is absorbed in the CIGS layer, rather than being reflected towards the sky. This can be mostly attributed to the refractive index mismatch between the glass cover and air, where a lot of the converted light which is emitted towards the top of the cell, is reflected back towards the cell.

In order to investigate the influence of the edge losses, the results of the AD method were also compared with MC simulations where a 150 x 150 mm solar cell was implemented, and the full surface of the cell was irradiated. The average absolute deviation between AD calculations and MC simulations is still below 1.5% and 1% when using 16 and 32 channels, respectively. It can be concluded that the light escaping though the sides of the cell has only a small influence on the results of the simulations.

#199984 - $15.00 USD Received 22 Oct 2013; revised 18 Jan 2014; accepted 26 Jan 2014; published 1 Apr 2014

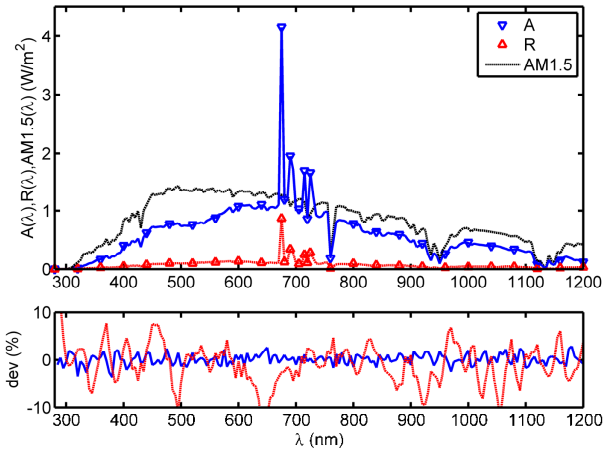

Fig. 4. Comparison between AD method (marks) and MC simulations (lines) of reflectance (R) and absorptance in the CIGS layer (A) of the encapsulated solar cell for an infinite solar cell, together with the incident irradiance on the cell (AM1.5 standard solar spectrum).

3.2 Computation time

The computations for the AD method and the MC simulations were performed on the same PC with Pentium Dual Core CPU E5700 3 GHz with 8 GB RAM memory. The operating system is Windows 7 64bit professional. The AD code was implemented in Matlab 7.1. The MC simulations were done using TracePro 7.3®.

The computation time strongly depends on the number of rays per wavelength used in the MC simulations and the number of channels considered in the AD method. Decreasing the number of rays (for the MC simulations) or channels (in the AD calculations) will lead to a shorter computation time but also to a lower accuracy. The amount of noise in the MC simulations can be quantified by performing different simulations with a different "seed" or initial random set of rays. In Fig. 5, the computation time and corresponding noise in the MC simulation is presented in function of the number of incident rays per wavelength, together with the accuracy and computation time of the AD method in function of the number of channels used for the calculations.

Setting the threshold accuracy to 1%, the MC simulation requires 5000 rays per wavelength, corresponding to approximately 1,7 h of computation time. The computation time of the AD method depends on the number of angular channels which are considered. If 32 channels are used, the computation time is approximately 8,5 minutes, if 16 channels are used, it is approximately 2 minutes. The short computation time for these AD calculations is remarkable taking into account the very wide excitation and emission spectrum, resulting in over 2000 conversion matrices to handle the fluorescence.

In conclusion, the AD method can be used to accurately simulate the reflected irradiance of the stack and the absorption in the semiconductor. The AD method reduces the computation time with a factor 12 using 32 channels, and a factor 52 using 16 channels, making the AD method better suited for optimization purposes than the MC simulations.

#199984 - $15.00 USD Received 22 Oct 2013; revised 18 Jan 2014; accepted 26 Jan 2014; published 1 Apr 2014

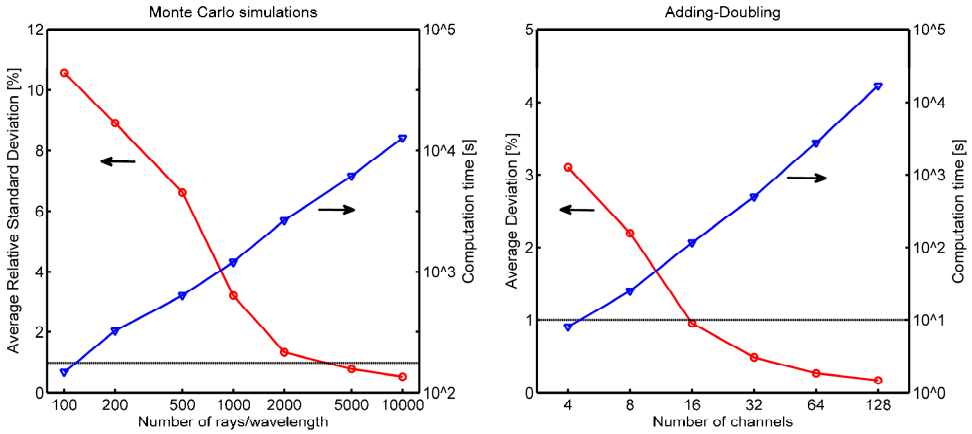

Fig. 5. Accuracy (red) and time computation (blue), in function of the number of incident wavelengths for the MC simulations (left) and in function of the number of channels for the AD calculations (right). The black lines denote the accuracy threshold of 1%.

4. Optimization of the luminescent down shifting layer

The AD method discussed in the previous sections can be used to optimize the LDS layer of the solar cell. The down-shifting layer changes the spectrum incident on the semiconductor, this will have the largest influence on the short-circuit current (I_{sc}), and only a small influence on the open-circuit voltage (V_{oc}), which is more dependent on material parameters than on the incident spectrum. The optimization parameter used here is the short-circuit current of the solar cell, which can be calculated using Eq. (1).

$$I_{sc} = \int A(\lambda) \cdot E(\lambda) \cdot S \cdot IQE(\lambda) \cdot \frac{\lambda}{h \cdot c} \cdot e \cdot d\lambda \qquad (1)$$

Herein, $A(\lambda)$ is the absorptance in the CIGS cell, $E(\lambda)$ is the incident solar irradiation (AM1.5 standard spectrum), S is the surface area of the solar cell, $IQE(\lambda)$ is the internal quantum efficiency of the CIGS cell (given in Fig. 3), h is Planck's constant, c is the speed of light, and e is the elementary charge. In the next sections, the LDS layer of the encapsulated solar cell is optimized to obtain the highest short-circuit current. To this extend, the absorptance in the semiconductor material $A(\lambda)$ will be calculated with the AD algorithm described above. The following optimization parameters will be considered: phosphor concentration and quantum yield (QY) of the fluorescent particles.

4.1 Optimization of the phosphor concentration

The phosphor concentration influences the absorption and scattering coefficient in a linear way. A higher concentration of phosphor will result in a higher absorptance of photons below 400 nm, where the IQE of the CIGS cell is zero. This light will be converted to wavelengths for which the CIGS cell is more efficient and this will increase the efficiency of the solar cell. On the other hand, increasing the phosphor concentration will also have some negative effects. The absorption in the LDS layer for wavelengths between 400 and 600 nm will increase and will give rise to additional losses if the QY is not 100%. Furthermore, a higher concentration of phosphor particles will also result in more scattering (the scattering coefficient increases linearly with the concentration). The phosphor particles cause scattering in all directions. The backwards scattered radiation will enhance the reflection of the stack and will not contribute to the generated current in the CIGS layer. The latter loss mechanism applies to all wavelengths, as opposed to the gain which only occurs at wavelengths below approximately 400 nm. In Fig. 6, the relative gain (compared to an encapsulated cell without

#199984 - $15.00 USD Received 22 Oct 2013; revised 18 Jan 2014; accepted 26 Jan 2014; published 1 Apr 2014

the phosphor) of the short-circuit current of the solar cell by increasing the phosphor concentration in the LDS layer is shown.

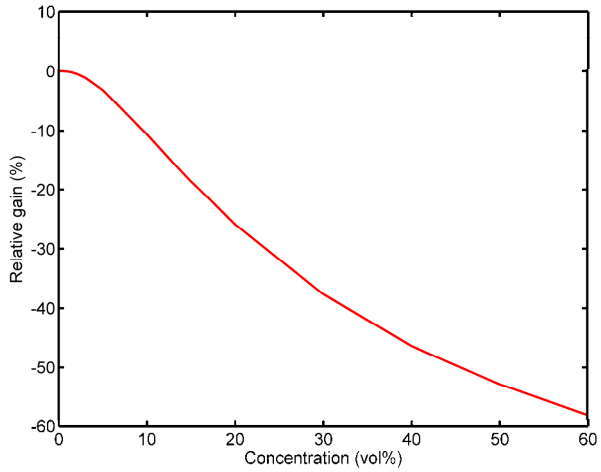

Fig. 6. Relative gain in I_{sc} by increasing the phosphor concentration in the LDS layer, with QY = 1 for the luminescent material.

From Fig. 6, it can be seen that no significant increase in the short circuit current can be expected using this phosphor as a down shifting material. This is caused by the fact that the phosphor particles are quite large which causes a lot of scattering ($\mu_s \approx 20.5$ mm^{-1}). The reflection "losses" due to the scattering quickly transcend the improvement in spectral response caused by the wavelength conversion.

4.2 Reduction of the scattering by the phosphor

The elastic scattering of the phosphor particles occurring in the LDS layer is caused by the difference in refractive index between the phosphor particles and the host medium. This problem can be solved by matching the refractive index of the host medium to the refractive index of the phosphor particles.

The refractive index of the host can be matched to the refractive index of the phosphor particles by choosing a different host material. A number of polymers exhibit a high refractive index, an overview of these materials can be found in ref [25]. These polymers may however not have the desired properties for solar applications.

A second approach to obtain a high refractive index polymer is to create a hybrid material also referred to as nanocomposite. The refractive index of such materials can be tuned by adding nanoparticles in the matrix. Under condition of uniform distribution of the particles and if the size of the nanoparticles is much smaller than the wavelengths of interest (2-5 nm), they don't distort the incident light wave and the light scattering is low [26]. The hybrid materials with a high concentration of nanoparticles can become effectively a homogeneous medium with a refractive index between the one of the polymer and the nanoparticles, the macroscopic effective refractive index of the hybrid material can be calculated using e.g. the Maxwell-Garnet Theory [27]. Commonly used materials to tune the refractive index of a polymer to obtain a transparent high refractive index layer are TiO2 and ZnS [28,29]. A refractive index of 1.7 could easily be obtained by e.g. mixing TiO2 (n≈2.5) nanoparticles in the EVA host medium [28].

The Lorenz-Mie calculations for the same particles in a host medium with refractive index 1.7 (instead of 1.5), result in a lower average scattering coefficient ($\mu_s \approx 16.0$ mm^{-1} instead of $\mu_s \approx 20.5$ mm^{-1}), and a higher average anisotropy factor ($g \approx 0.996$ instead of $g \approx 0.905$), indicating the scattering occurs now much more in the forward direction.

#199984 - $15.00 USD Received 22 Oct 2013; revised 18 Jan 2014; accepted 26 Jan 2014; published 1 Apr 2014

Under these new conditions, the simulations from section 4.1 are repeated. The improvement in the short-circuit current (compared to the original encapsulated cell with non-matched layer without phosphor) with increasing phosphor concentration is shown in Fig. 7. A totally different behavior can be observed now. For a phosphor with unity quantum yield, the optimum concentration is 28%, and an increase in I_{sc} of 4.3% can be expected. For a phosphor with QY = 0.95, the optimum concentration is 25% and the increase in I_{sc} is 3.0%. For a QY = 0.90, the optimum concentration is lowered to 20% and the increase in I_{sc} is limited to 1.7%.

From Fig. 7, it can also be noted that at 0% concentration, I_{sc} is lower than for the original cell (without matching the refractive index of the LDS layer to the phosphor). This can be explained by additional Fresnel reflections occurring in the multi-layer EVA encapsulation.

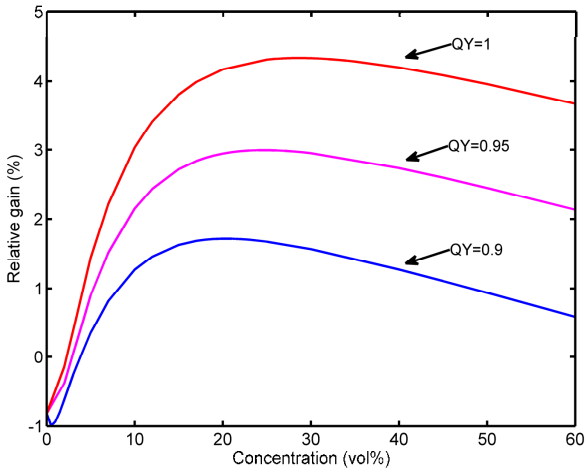

Fig. 7. Relative gain in I_{sc} by increasing the phosphor concentration under conditions of a matched refractive index for different QY values for the luminescent material.

These losses can be minimized by adapting the refractive index of the top and bottom layer of the EVA multilayer. To minimize Fresnel reflections, the top layer should have a refractive index n≈1.6, the bottom layer should have a refractive index n≈1.7, identical to the refractive index of the down-shifting layer. The simulation results are shown in Fig. 8. I_{sc} at 0% concentration is now slightly higher than for the original solar cell (without matching the refractive index of any layer), an increase in I_{sc} of 0.62% can be expected . The maximum increase in I_{sc} is found at concentrations equal to 28% (I_{sc} + 9.0%), 25% (I_{sc} + 7.4%) and 22% (I_{sc} + 6.0%) for a QY of the phosphor unity, 0.95 and 0.9, respectively.

4.3 Impact of the QY of the phosphor

In the previous section, only high QY values were considered. In Fig. 9, the maximum possible relative increase of the short-circuit current (compared to the cell with matched refractive indices and phosphor concentration 0%) is presented for a broad range of QY values. For each QY value, the increase is calculated under the condition of optimized concentration, which is also indicated in Fig. 9. The calculations were performed for the EVA multi-layer with matched refractive indices for all layers.

#199984 - $15.00 USD Received 22 Oct 2013; revised 18 Jan 2014; accepted 26 Jan 2014; published 1 Apr 2014

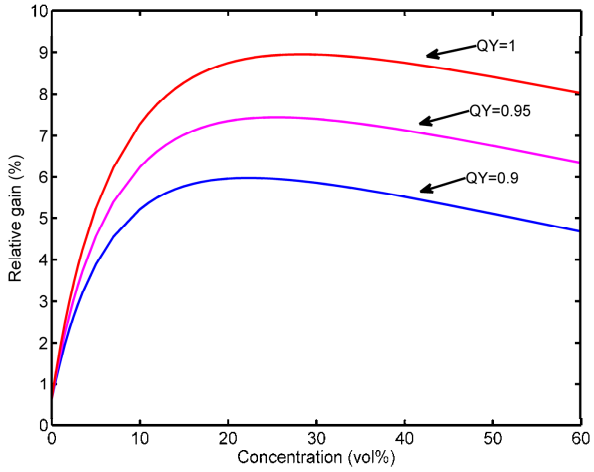

Fig. 8. Relative gain in I_{sc} by increasing the phosphor concentration under conditions of a matched refractive index and reduced Fresnel reflection in the multi-layer for different QY values for the luminescent material.

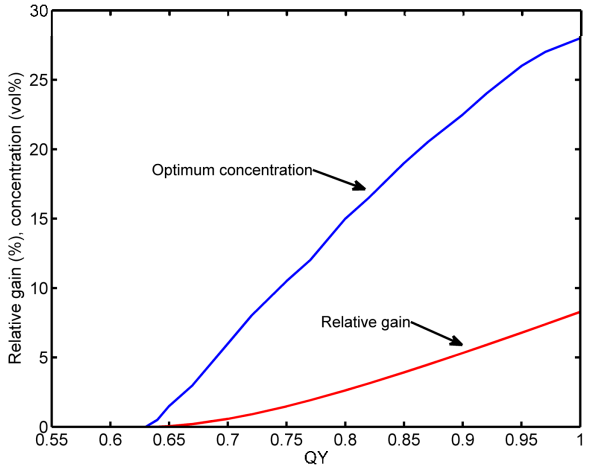

Fig. 9. Maximum increase of the I_{sc} and the concentration ρ of phosphor where the maximum occurs in function of the QY of the phosphor.

From Fig. 9, it can be seen that the minimum required quantum yield for this particular phosphor to obtain a positive effect on the photocurrent is 0.64. The optimum concentration for the phosphor increases with increasing QY. A trade of between the loss mechanisms, i.e. the scattering and the losses due to non-unity QY of the phosphor, and the gain (due to conversion of the radiation below 400 nm to above 600 nm) occurs. Since there is an overlap between the excitation spectrum of the phosphor and the high IQE wavelength range of the cell, radiation converted with low efficiency will create less electron-hole pairs than if no down-shifting layer was present, thus causing extra losses in this wavelength range. If the concentration is too high, or the QY too low, these losses may transcend the gain due to the conversion of the radiation below 400 nm. This explains why the optimum concentration increases for a higher QY.

In this configuration, where the refractive index of the host material is matched to the phosphors refractive index, reflection losses due to scattering play only a minor roll.

#199984 - $15.00 USD Received 22 Oct 2013; revised 18 Jan 2014; accepted 26 Jan 2014; published 1 Apr 2014

However, they are still present and explain why the I_{sc} decreases again at very high concentrations (see also Figs. 7 and 8) and thus an optimum concentration can be found. At these optimum concentrations, it is no longer beneficial to add more phosphor since most of the light below 400 nm is already absorbed (e.g. at ρ = 11vol%, less than 10% of the light below 400 nm reaches the semiconductor). The scattering losses however still increase with a higher concentration of phosphor.

Further improvements in the LDS layer could be made by selecting a phosphor for which the narrow excitation band falls entirely below the IQE wavelength range. By selecting a fluorescent material with smaller particles, such as dyes or quantum dots [1,6], the scattering and thus reflection losses can further be reduced, even without the need of taking precautions to match the refractive index of the host and fluorescent material.

5. Conclusions

In this paper, the adding-doubling method was successfully applied for the optical simulation of a solar cell stack having a planar luminescent down shifting layer. The results obtained with the AD method were compared to the results obtained with Monte Carlo simulations. The average relative deviation was lower than 1% and 1.5% when using respectively 32 and 16 channels in the AD method. The AD method however, only required 8,5 and 2 minutes computation time for 32 and 16 channels, respectively, while the MC method required 1,7 hours to obtain similar accuracy. The short computation time and high accuracy makes the AD method well suited for optimization purposes.

Applying this method, the optimum concentration of SrB_4O_7:5%Sm^{2+},5%Eu^{2+} as a down shifting phosphor was investigated. If no precautions are taken to reduce the scattering originating from the phosphor particles, no significant improvement in the short-circuit current of the encapsulated cell can be obtained. When reducing the scattering by matching the refractive index of the host material to the refractive index of the phosphor particles, a maximum improvement in the short-circuit current of the encapsulated cell of 9.0% and 6.0% can be made for a QY of the phosphor of 1 and 0.9, respectively. This indicates that SrB_4O_7:5%Sm^{2+},5%Eu^{2+} is an interesting phosphor for CIGS solar cells, since previous studies on LDS layers for CIGS cells showed only an increase of 1-4% [2,9].

Furthermore it was found that the QY of the phosphor must be at least 0.64 in order to generate a positive effect. This rather low value can be explained by the fact that there is only a small overlap between the excitation spectrum of the phosphor and the spectral IQE range of the CIGS solar cell.

Appendix

The adding-doubling (AD) method calculates the reflectance and transmittance through layered media, assuming the reflection and transmission characteristics of each separate layer are known. The first step is to calculate the reflection and transmission characteristics of each layer separately. For this purpose, the angular distribution of the radiance within a layer is described using a definite number of channels, each corresponding to a cone confined by the polar angles θ_n and θ_{n+1}. The flux incident on the material is divided into angular subdivisions, called channels, and can be written as a vector, where each element in the vector represents the flux within the channel. The reflection and transmission properties of the layer are written as a matrix, describing how each channel can receive radiation from and distribute to other channels [12]. Indeed, for scattering and fluorescent layers, the radiance in one channel will be redistributed into other channels when passing through the layer. For light travelling in non-scattering and non-fluorescent layers, the transmission and reflection matrices will be a diagonal matrix, since no light will be distributed from one channel to another [12].

The reflection and refraction occurring at the interface between two media is treated as a separate ‘layer’, and each interface has its own reflection and transmission matrices. Light travelling from media with refractive index n_1 to a medium with refractive index n_2 will be refracted according to Snell’s law. Since this is valid for the radiance in each channel, the radiances are not transferred to another channel, but the polar angle of each channel is

#199984 - $15.00 USD Received 22 Oct 2013; revised 18 Jan 2014; accepted 26 Jan 2014; published 1 Apr 2014

adjusted. One can think of this as bending the channels instead of transferring the radiance from one channel to another. The reflectance and transmittance is calculated using the Fresnel equations and gathered in a diagonal matrix [14].

In the case of scattering layers, the transmission and reflection matrices of a layer are determined by solving the radiative transfer equation (RTE), given by Eq. 2.

$$\mathbf{s}\nabla L(\mathbf{r},\mathbf{s}) = -(\mu_a + \mu_s)L(\mathbf{r},\mathbf{s}) + \mu_s \int_{4\pi} p(\mathbf{s},\mathbf{s}')L(\mathbf{r},\mathbf{s}')d\Omega' \tag{2}$$

Herein, $L(\mathbf{r},\mathbf{s})$ is the radiance at position **r** and direction **s**, **s'** is the scattered direction, μ_a and μ_s are respectively the absorption and scattering coefficient, $p(\mathbf{s},\mathbf{s}')$ is the phase function, which determines the angular distribution of the light after a single scatter event. The RTE is solved for a thin 'single scatter' layer for each wavelength interval, assuming that the optical properties of the layer are homogeneous, the layer is plane parallel and has infinite lateral dimensions and the incident beam is azimuthally symmetric. A more elaborate discussion on how the reflection and transmission matrices are obtained from the RTE can be found in [12].

In the case of fluorescent layers, the excitation and emission wavelength region are divided into a discrete number of wavelength intervals. The RTE is extended for each emission wavelength interval, given by Eq. 3 [17].

$$\begin{aligned}\mathbf{s}\nabla L(\mathbf{r},\mathbf{s}) &= -(\mu_a + \mu_s)L(\mathbf{r},\mathbf{s}) + \mu_s \int_{4\pi} p(\mathbf{s},\mathbf{s}')L(\mathbf{r},\mathbf{s}')d\Omega' \\ &+ w_M \sum_{i=1}^{N} \left\{ \mu_e(\lambda_i) QY \frac{1}{4\pi} \int_{4\pi} L(\mathbf{r},\mathbf{s}',\lambda_i)d\Omega'\Delta\lambda \right\}\end{aligned} \tag{3}$$

The third term on the right hand side of Eq. 3 is the contribution at the emission wavelength interval due to fluorescence. In Eq. 3, $L(\mathbf{r},\mathbf{s}',\lambda_i)$ is the radiance at the excitation wavelength interval with central wavelength λ_i, $\mu_e(\lambda_i)$ is the excitation coefficient, QY is the quantum yield of the fluorescent material, The factor w_M denotes the fraction of the selected emission wavelength interval in the emission spectrum and can be immediately derived from the emission spectrum. Each excitation wavelength has a contribution at the emission wavelength [17].

Several solutions exist to solve the (fluorescent) RTE, e.g. Monte Carlo simulations [30], two flux approximations [31], discrete ordinates angular discretization schemes (S_N methods) [32], and the AD method discussed in this study. The latter approach has the advantage that it combines fast computation with high accuracy.

In the AD method, the redistribution of radiation due to fluorescence is denoted in a conversion matrix, converting radiances from each excitation wavelength interval to the emission wavelength intervals. The number of conversion matrices needed is equal to the product of the number of excitation wavelength intervals and the number of emission wavelength intervals. The conversion matrices also redistribute the radiances angularly, since the fluorescence occurs isotropically. A more elaborate discussion on how the conversion matrices are obtained from the RTE can be found in [17].

Once all the necessary matrices are determined for the separate layers, these separate layers can be combined to determine the transmission and reflection characteristics of a combination of layers until the desired thickness of the macroscopic layer is reached [12].

Starting from two separate layers or interfaces, the reflection and transmission characteristics of the combination of both layers are calculated using Eq. 4 and 5 [12].

$$\mathbf{R}_{20}(\lambda) = \mathbf{R}_{21}(\lambda) + \mathbf{T}_{12}(\lambda)(\mathbf{E} - \mathbf{R}_{10}(\lambda)\mathbf{R}_{12}(\lambda))^{-1}\mathbf{R}_{10}(\lambda)\mathbf{T}_{21}(\lambda) \tag{4}$$

$$\mathbf{T}_{02}(\lambda) = \mathbf{T}_{12}(\lambda)(\mathbf{E} - \mathbf{R}_{10}(\lambda)\mathbf{R}_{12}(\lambda))^{-1}\mathbf{T}_{01}(\lambda) \tag{5}$$

Herein, **E** is the unity matrix. $\mathbf{R}_{xy}(\lambda)$ and $\mathbf{T}_{xy}(\lambda)$ are the reflection and transmission matrices for a layer confined between interface x and y, with the incoming light incident on interface x. The first layer is defined by interface 0 and 1, the second layer by interfaces 1 and

#199984 - $15.00 USD Received 22 Oct 2013; revised 18 Jan 2014; accepted 26 Jan 2014; published 1 Apr 2014

2. The fluorescent conversion matrices for two joint layers can be calculated with Eqs. 6 and 7 [17].

$$\mathbf{R}^{c}_{20}\left(\lambda_i^X,\lambda_j^M\right)=$$
$$\mathbf{T}_{12}(\mathbf{E}-\mathbf{R}_{10}\mathbf{R}_{12})^{-1}\left[\begin{array}{l}\mathbf{R}_{10}\left(\begin{array}{l}\mathbf{R}^{c}_{12}\left(\lambda_i^X,\lambda_j^M\right)\left\{\begin{array}{l}\left[\mathbf{E}-\mathbf{R}^{c}_{10}\left(\lambda_i^X,\lambda_j^M\right)\mathbf{R}^{c}_{12}\left(\lambda_i^X,\lambda_j^M\right)\right]^{-1}\\ \mathbf{R}^{c}_{10}\left(\lambda_i^X,\lambda_j^M\right)\mathbf{T}^{c}_{21}\left(\lambda_i^X,\lambda_j^M\right)\end{array}\right\}\\ +\mathbf{T}^{c}_{21}\left(\lambda_i^X,\lambda_j^M\right)\end{array}\right)\\ +\mathbf{R}^{c}_{10}\left(\lambda_i^X,\lambda_j^M\right)\left[\mathbf{E}-\mathbf{R}^{c}_{12}\left(\lambda_i^X,\lambda_j^M\right)\mathbf{R}^{c}_{10}\left(\lambda_i^X,\lambda_j^M\right)\right]^{-1}\mathbf{T}_{21}\left(\lambda_i^X\right)\end{array}\right]$$
$$+\mathbf{R}^{c}_{21}\left(\lambda_i^X,\lambda_j^M\right)+\mathbf{T}^{c}_{12}\left(\lambda_i^X,\lambda_j^M\right)\left[\mathbf{E}-\mathbf{R}_{10}\left(\lambda_i^X\right)\mathbf{R}_{12}\left(\lambda_i^X\right)\right]^{-1}\mathbf{R}_{10}\left(\lambda_i^X\right)\mathbf{T}_{21}\left(\lambda_i^X\right)$$
(6)

$$\mathbf{T}^{c}_{02}\left(\lambda_i^X,\lambda_j^M\right)=$$
$$\mathbf{T}_{12}(\mathbf{E}-\mathbf{R}_{10}\mathbf{R}_{12})^{-1}\left\{\begin{array}{l}\mathbf{R}_{10}\mathbf{R}^{c}_{12}\left(\lambda_i^X,\lambda_j^M\right)\left[\mathbf{E}-\mathbf{R}_{10}\left(\lambda_i^X\right)\mathbf{R}_{12}\left(\lambda_i^X\right)\right]^{-1}\mathbf{T}_{01}\left(\lambda_i^X\right)\\ +\mathbf{R}^{c}_{10}\left(\lambda_i^X,\lambda_j^M\right)\left[\mathbf{E}-\mathbf{R}_{12}\left(\lambda_i^X\right)\mathbf{R}_{10}\left(\lambda_i^X\right)\right]^{-1}\mathbf{R}_{12}\left(\lambda_i^X\right)\mathbf{T}_{01}\left(\lambda_i^X\right)\\ +\mathbf{T}^{c}_{01}\left(\lambda_i^X,\lambda_j^M\right)\end{array}\right\}$$
$$+\mathbf{T}^{c}_{12}\left(\Delta\lambda_i^X,\Delta\lambda_j^M\right)\left[\mathbf{E}-\mathbf{R}_{10}\left(\Delta\lambda_i^X\right)\mathbf{R}_{12}\left(\Delta\lambda_i^X\right)\right]^{-1}\mathbf{T}_{01}\left(\Delta\lambda_i^X\right)$$
(7)

$\mathbf{R}^{c}_{xy}(\lambda^{X}_{i},\lambda^{M})$ and $\mathbf{T}^{c}_{xy}(\lambda^{X}_{i},\lambda^{M})$ are the fluorescent conversion matrices, converting the light from excitation wavelength interval with central wavelength λ^{X}_{i} to the emission wavelength interval with central wavelength λ^{M}. The matrices $\mathbf{T}_{xy}$ and $\mathbf{R}_{xy}$ are the regular (non-conversion) reflection and transmission matrices for non-fluorescent purposes.

Acknowledgments

The authors would like to thank the SIM (Flemish Strategic Initiative for Materials) and IWT (Flemish agency for Innovation by Science and Technology) for their financial support through the SoPPoM project within the SIBO program.

#199984 - $15.00 USD Received 22 Oct 2013; revised 18 Jan 2014; accepted 26 Jan 2014; published 1 Apr 2014